TISSUE ENGINEERING: Part A
Volume 25, Numbers 3 and 4, 2019

DOI: 10.1089/ten.tea.2018.0046

termis
Tissue Engineering
& Regenerative Medicine
International Society

ORIGINAL ARTICLE

Regeneration of Osteochondral Defects Using Developmentally Inspired Cartilaginous Templates

Susan Critchley, PhD,[1,2] Gráinne Cunniffe, PhD,[1,2] Adam O'Reilly, PhD,[1,2] Pedro Diaz-Payno, MSc,[1,2] Rossana Schipani, MSc,[1,2] Aidan McAlinden, MVB, MSc,[3] Daniel Withers,[4] Jungyoun Shin, PhD,[5] Eben Alsberg, PhD,[5–7,*] and Daniel J. Kelly, PhD[1,2,8,9]

There is increased interest in recapitulating aspects of development when designing new tissue engineering strategies. Long bones and their epiphyses are formed through endochondral ossification, a process by which a cartilage template develops in response to genetic and environmental cues to generate a bone organ. The objective of this study was to evaluate the capacity of engineered cartilage templates to regenerate osteochondral (OC) defects created in the femoral condyle of skeletally mature rabbits. To this end, bone marrow-derived mesenchymal stem cells (BMSCs) were encapsulated in RGD (arginine/glycine/aspartic acid)-functionalized, γ-irradiated alginate hydrogel and chondrogenically primed *in vitro* to engineer cartilage templates tailored for OC defect regeneration. While comparable levels of healing were observed in the bony region of empty and treated groups, the quality of healing was notably different in the chondral region of these defects. Mechanical testing revealed that treatment with engineered cartilage templates promoted the development of a stiffer repair tissue at the articular surface, which correlated with histomorphometric analysis demonstrating the formation of a more hyaline cartilage-like repair tissue. Next, a computational mechanobiological model was used to better understand how local environmental cues were regulating the regenerative process *in vivo*. This model predicted that higher strains and lower levels of oxygen in the chondral region of the defect were preventing cartilage template progression along the endochondral pathway, with hyaline cartilage or fibrocartilage eventually forming depending on local strain magnitudes. In contrast, higher levels of oxygen and lower magnitudes of strain in the osseous region of the defect facilitated progression of the engineered cartilage template along an endochondral pathway. In conclusion, this study demonstrates that engineered cartilage templates can enhance OC defect regeneration, pointing to the potential for developmentally inspired soft tissue templates, engineered using BMSCs, to regenerate damaged and diseased joints.

Keywords: hydrogel, mesenchymal stem cell, endochondral, chondrogenesis, osteochondral, finite element model

Impact Statement

Successfully treating osteochondral defects involves regenerating both the damaged articular cartilage and the underlying subchondral bone, in addition to the complex interface that separates these tissues. In this study, we demonstrate that a cartilage template, engineered using bone marrow-derived mesenchymal stem cells, can enhance the regeneration of such defects and promote the development of a more mechanically functional repair tissue. We also use a computational mechanobiological model to understand how joint-specific environmental factors, specifically oxygen levels and tissue strains, regulate the conversion of the engineered template into cartilage and bone *in vivo*.

[1]Trinity Centre for Bioengineering, Trinity Biomedical Sciences Institute, Trinity College Dublin, Dublin, Ireland.
[2]Department of Mechanical and Manufacturing Engineering, School of Engineering, Trinity College Dublin, Dublin, Ireland.
[3]Section of Veterinary Clinical Studies, School of Veterinary Medicine, University College Dublin, Dublin, Ireland.
[4]Sports Surgery Clinic, Dublin, Ireland.
Departments of [5]Biomedical Engineering and [6]Orthopaedic Surgery, Case Western Reserve University, Cleveland, Ohio.
[7]National Centre for Regenerative Medicine, Case Western Reserve University, Cleveland, Ohio.
[8]Advanced Materials and Bioengineering Research Centre, Trinity College Dublin and Royal College of Surgeons in Ireland, Dublin, Ireland.
[9]Department of Anatomy, Royal College of Surgeons in Ireland, Dublin, Ireland.
**Current affiliation:* Departments of Bioengineering and Orthopaedic Surgery, University of Illinois, Chicago, IL.

Introduction

Successfully treating osteochondral (OC) defects involves regenerating both the damaged articular cartilage and the underlying subchondral bone, in addition to the complex interface that separates these tissues. Current treatments such as mosaicplasty are limited by complications such as donor-site morbidity, matching the topography of the damaged site, and poor graft integration.[1–3] This has motivated the development of tissue-engineered implants to treat these clinically challenging defects.[4,5] To this end, there has been increased interest in recapitulating aspects of tissue or organ development when designing new regenerative strategies. All long bones, including their epiphyses, are formed, in part, by the process of endochondral ossification.[6,7] Their development involves the condensation of stem cells, which differentiate into chondrocytes to form a cartilage model/template. The chondrocytes enlarge and become hypertrophic, secreting collagen type X and angiogenic factors, and their surrounding extracellular matrix (ECM) is invaded by vasculature.[8] The subsequent delivery of oxygen, growth factors, and other regulatory cues through this vasculature, as well as the recruitment of osteoprogenitor cells, promotes osteogenesis and bone formation.[9] During postnatal development, articular cartilage also acts as a surface growth plate for the longitudinal, radial, and lateral growth of the epiphyseal bone.[6] Therefore, cartilage acts as the precursor tissue to the cancellous bone, subchondral bone, calcified cartilage, and articular cartilage that make up a mature long bone organ. Bone marrow-derived mesenchymal stem cells (BMSCs) have been used to engineer both articular cartilage[10–12] and hypertrophic cartilage templates for endochondral bone tissue engineering.[7,13–15] Under appropriate environmental conditions, this suggests that cartilage tissue engineered using BMSCs could provide a template for the development of the different components of the OC unit. To date, no tissue engineering strategy exists to successfully regenerate the complex bone and articular and calcified cartilage interface within damaged joints.

While it is well established that cartilaginous tissues engineered using BMSCs can progress along the endochondral pathway and mineralize,[7,13,16,17] certain environmental factors such as oxygen,[18–20] or the application of joint-like mechanical loading,[21–23] can modulate this process and promote the development of a more stable chondrogenic phenotype. *In situ,* the oxygen tension of bone ranges from 5% to 12.5% pO_2, whereas cartilage resides in a more hypoxic environment with levels ranging from 1% to 5% pO_2.[24] BMSC-laden constructs maintained at or below 5% pO_2 undergo enhanced chondrogenesis with a suppression of hypertrophy, whereas culture at higher oxygen concentrations tends to direct BMSCs toward an osteogenic lineage.[19,25,26] Physiological levels of hydrostatic pressures increase transforming growth factor-β (TGF-β) expression, regulate ECM synthesis,[21,27–29] and suppress calcium deposition within BMSC-laden constructs,[22,30] however, application of levels outside the physiological range can have negative effects.[27] Other mechanical cues such as dynamic compression can also enhance chondrogenesis of MSCs and suppress their tendency to progress along an endochondral pathway.[21,30,31,32] It would be reasonable to conclude that such environmental cues will also play a central role in determining the fate of tissues engineered using BMSCs once they are implanted *in vivo*.

Cartilage and bone tissue engineering strategies often involve the encapsulation of cells into hydrogels, providing them a niche to proliferate and/or differentiate into tissue-specific cells. Alginate is a naturally derived, biocompatible hydrogel that supports cell differentiation and ECM synthesis and is often used in bone and cartilage tissue engineering.[33–41] It does not contain specific ligands for cell adhesion; however, introducing peptides such as the arginine/glycine/aspartic acid (RGD) sequence has been shown to facilitate cellular adhesion. This has been shown to support cellular proliferation, an osteogenic phenotype,[42] and promote endochondral bone formation.[14] Alginate is generally slow to degrade, which can be a limitation for bone development, as vascularization and the subsequent delivery of nutrients can be impeded or inhibited.[39] Strategies to accelerate degradation include altering the molecular weight through γ-irradiation and/or oxidation of the material,[42–44] shown to enhance the capacity of these hydrogels to support tissue regeneration.[40,45]

The first objective of this study was to tissue engineer a cartilage template using BMSCs and to then evaluate its capacity to repair a critically sized OC defect in the femoral condyle of skeletally mature rabbits. To this end, BMSCs were encapsulated in an RGD-functionalized, γ-irradiated alginate hydrogel and chondrogenically primed *in vitro* to engineer cartilage templates tailored for OC defect regeneration. Our hypothesis was that this cartilage template would undergo spatially defined differentiation *in vivo* in response to the unique environmental conditions within an OC defect, resulting in the development of a repair tissue consisting of hyaline articular cartilage overlying a layer of bone formed via endochondral ossification. A computational mechanobiological model was then used to elucidate the environmental and mechanical conditions *in vivo* to provide further insight into the factors regulating the repair tissue phenotype.[46,47]

Materials and Methods

Cell isolation and expansion

BMSCs were obtained from the femur of 4- to 6-month-old lapine donors. Bone marrow was removed from the femoral shaft and washed in high-glucose Dulbecco's modified Eagle's medium (hgDMEM, GlutaMAX™; Biosciences, Ireland) supplemented with 8% fetal bovine serum (Biosciences), 2% rabbit serum (Sigma, Ireland), 1% penicillin (100 U/mL), and streptomycin (100 μg/mL; Biosciences). A homogenous cell suspension was achieved by triturating with an 18G needle. The solution was centrifuged twice at 650 *g* for 5 min, with removal of the supernatant. The resultant cell pellet was triturated and the cell suspension was filtered through a 40 μm cell sieve before plating at a density of 5×10^3 cells/cm^2. Following colony formation, cells were trypsinized, counted, and replated for further passage at a density of 5×10^3 cells/cm^2. All expansion was conducted at 5% oxygen tension and media were changed twice weekly. Cells were embedded within the alginate gel at the end of passage 2.

Engineering of the cartilage template

The cartilage template was prepared by dissolving RGD-γ alginate in sterile hgDMEM to make up a final concentration

of 1.5% w/v. RGD-γ alginate was made as follows: low-molecular-weight sodium alginate (52,000 g/mol) was prepared by irradiating Protanal LF 20/40 (196,000 g/mol; FMC Biopolymer, Philadelphia, PA) at a gamma dose of 5 mrad.[45] RGD-modified alginates were prepared by coupling the GGGGRGDSP to the alginate by carbodiimide reaction chemistry. Alginate (10 g) was dissolved at 1% (w/v) in MES buffer (pH 6.5). Sulfo-NHS (274 mg; Pierce, Rockford, IL), 1-ethyl-3-(3-dimethylaminopropyl)carbodiimide (484 mg; Sigma), and GGGGRGDSP peptide (100 mg; AI-BioTech, Richmond, VA) were then added to the alginate solution. After reacting for 24 h at 48°C, the reaction was stopped by addition of hydroxylamine (0.18 mg/mL; Sigma), and the solution was purified by dialysis against ultrapure deionized water (MWCO 3500; Spectrum Laboratories, Rancho Dominguez, CA) for 3 days, treated with activated charcoal (0.5 mg/100 mL, 50–200 mesh; Fisher, Pittsburgh, PA) for 30 min, filtered (0.22 mm filter), and lyophilized.[48–50] The constructs were formed by combining BMSCs, counted, and spun to form a cell pellet, with the alginate, using a 16G needle to mix the suspension with a final density of 2×10^7 cells/mL. The alginate/cell suspension was poured into a specifically designed 4% agarose mold containing 50 mM $CaCl_2$ and allowed to crosslink for 30 min at 37°C to produce 4×4 mm cylindrical constructs. Constructs were maintained in chondrogenic medium, consisting of hgDMEM supplemented with penicillin (100 U/mL)/streptomycin (100 μg/mL), 100 μg/mL sodium pyruvate, 40 μg/mL L-proline, 50 μg/mL L-ascorbic acid-2-phosphate, 1.5 mg/mL bovine serum albumin, 1×insulin/transferrin/selenium, 100 nM dexamethasone (all from Sigma-Aldrich, Ireland), and 10 ng/mL recombinant human TGF-β3 (ProSpec-Tany TechnoGene Ltd., Israel). Constructs were cultured at 37°C with 5% oxygen for 32 days with medium exchange twice weekly.

Biochemical analysis

Constructs were digested in papain (125 μg/mL) in 0.1 M sodium acetate, 5 mM cysteine HCl, and 50 mM EDTA (pH 6.0; all from Sigma-Aldrich) at 60°C under constant rotation for 18 h. Total DNA content was quantified using the Hoechst bisbenzimide 33258 dye assay (Sigma-Aldrich). Proteoglycan content was estimated by quantifying the amount of sulfated glycosaminoglycan (sGAG) in constructs using the dimethylmethylene blue dye-binding assay (Blyscan, Biocolor Ltd.), with a chondroitin sulfate standard. Total collagen content was determined by measuring the hydroxyproline content. Samples were hydrolyzed at 110°C for 18 h in concentrated HCL (38%) and assayed using a chloramine-T assay with a hydroxyproline-to-collagen ratio of 1:7.69.[51]

Cartilage template implantation

New Zealand white (6–8 months) rabbits were anesthetized with ketamine/medetomidine maintained using isoflurane and oxygen. The surgical sites were prepared by shaving and washing with chlorhexidine surgical scrub and alcohol. Surgical drapes were used to isolate the surgical sites. Defects (4×4 mm in diameter) were introduced in the medial femoral condyle of the hind leg using a biopsy punch and a surgical burr. The defects were lavaged with saline before implanting the cartilage template. Two defects were made per rabbit (one in each femur), constructs were implanted ($n=6$) by press-fitting, and empty defects served as controls ($n=6$). Postsurgery, rabbits were permitted free activity with postoperative analgesia buprenorphine hydrochloride, given for 3 days. Animals were sacrificed after 3 months using pentobarbital. This protocol and study were reviewed and approved by the Ethics Committee of Trinity College Dublin, Ireland.

Histology and immunochemistry

Constructs were fixed in 10% formalin (Sigma-Aldrich) for 48 h. They were decalcified using "Decalcifying Solution-Lite" (Sigma-Aldrich), then dehydrated through graded alcohols, embedded in paraffin, and sliced to 10 μm. Slices were stained with 1% alcian blue 8GX (Sigma-Aldrich) in 0.1 M HCl, pH 1 for sGAG, or with aldehyde fuchsin and 1% alcian blue, pH 1. Collagen types I, II, and X were evaluated using a standard immunohistochemical technique; sections were rehydrated and treated with chondroitinase ABC (Sigma-Aldrich) in a humidified environment at 37°C to enhance permeability of the ECM. This was followed by incubation in goat serum to block nonspecific sites and the relevant primary antibodies (mouse monoclonal; Abcam); collagen type I (ab90395, 1:400), collagen type II (ab3092, 1:100), or collagen type X (ab49945, 1:100) was applied overnight at 4°C. Treatment with peroxidase preceded the application of the secondary antibody (collagen type I and II, B7151, 1.5:200; collagen type X, ab49760, 1:200) at room temperature for 1 h. Thereafter, all sections were incubated with ABC reagent (Vectastain PK-400; Vector Labs) for 45 min. Finally, sections were developed with DAB peroxidase (Vector Labs) for 5 min. Positive and negative controls were included in the immunohistochemical staining protocols.

Histological scoring

Histological and macroscopic blind scoring was conducted by six impartial people in groups of two ($n=3$ scores). The wax-embedded sample was cut down the center and sliced from the center of the defect. Two histological slides (one from each side of the sample) were included in the randomly selected histological slides for scoring, and an average score was calculated. Histological and macroscopic images were scored using a modified version of the O'Driscoll score (Tables 1 and 2).

Mechanical testing

Indentation tests were performed using a single column Zwick (Zwick, Roell, Germany) with a 5 N load cell. Unconfined compression tests were carried out as previously described.[52] Briefly, the repaired tissue was indented using an impermeable metal indenter of 1 mm diameter to a depth of 50 μm into the

Table 1. Macroscopic Scoring

Surface smoothness of the cartilage surface	
Smooth	0
Moderate	1
Irregular	2
Severe	3
Edge integration with native cartilage	
Completely integrated	0
Partial	1
None	2

tissue and held until relaxation. Subsequently, a dynamic test was performed at 1 Hz, from this the amplitude of the dynamic stress was extracted by dividing by the average force between the peak and trough of 10 cycles by the cross-sectional area (CSA). The mechanics of the repair tissue was assessed at the center point, unless there was an uneven surface; in such cases, preference was given to the region with the most repair tissue slightly left or right of the center of the defect site.

Microcomputed tomography

Microcomputed tomography (μCT) scans were performed on the femoral condyle explants using a Scanco Medical 40 μCT system (Scanco Medical, Bassersdorf, Switzerland) to visualize and quantify mineral deposition. Six condyles were scanned per experimental and control group after 3 months *in vivo*. Constructs were scanned in 50% EtOH, at a voxel resolution of 30 μm, a voltage of 70 kVp, and a current of 114 μA. Reconstructed three-dimensional (3D) images were generated to visualize the repaired bone. Quantification of mineralization within the defect site was performed by setting a threshold of 210 (corresponding to a density of 399.5 mg hydroxyapatite/cm^3) and calculating the bone volume within a 3.5×3.5 mm cylinder, which excluded the original bone.

Table 2. Histological Scoring

% Repair tissue that is hyaline	
80–100	8
60–80	6
40–60	4
20–40	2
0–20	0
Articular surface continuity	
Continuous and smooth	2
Continuous but rough	1
Discontinuous	0
Thickness of repair tissue compared with host cartilage	
81–120% of normal cartilage	2
51–81% of normal cartilage	1
0–50% of normal cartilage	0
Tidemark	
Present	2
Incomplete	1
Absent	0
Integration of cartilage	
Complete (integrated on both sides)	2
Partial	1
Poor (not integrated)	0
Degenerative changes in the repair tissue	
Normal cellularity	2
Slight to moderate hypocellularity or hypercellularity	1
Severe hypocellularity or hypercellularity	0
Degenerative changes in adjacent cartilage	
Normal cellularity, no clusters, no fibrillations	3
Normal cellularity, mild clusters, superficial fibrillations	2
Mild cellularity, moderate fibrillations	1
Severe changes in cellularity, moderate fibrillations	0
Chondrocyte clustering	
No clusters	2
<25% of cells	1
25–100% of cells	0
Total score	23

Computational modeling

A previously developed computational model was used to predict BMSC differentiation and tissue development in the empty and treated defect.[46,47,53,54] This model utilized an iterative procedure outlined in greater detail in a previous study.[54] Briefly, a finite element model was used to determine the mechanical environment within the defect (Fig. 1a). The dimensions and loading conditions of the condyle were obtained from the literature.[55–58] Angiogenesis and BMSC migration and proliferation were modeled using a lattice-based approach.[59] Similar to previous studies, blood vessel growth was biased in the direction of the minimum principal strain.[47,53] The results of the angiogenesis and cell migration models were then used as inputs to an oxygen diffusion model. In this case, oxygen consumption from the cells was modeled using Michaelis–Menten kinetics.[47–53] Cell differentiation was predicted using a previously developed algorithm, which assumed that the fate of BMSCs was dependent on the local oxygen tension and substrate stiffness,[60–62] while the fate of cartilage was influenced by the local oxygen tension and octahedral shear strain (Fig 1b, c). Of note for this study is that cartilage can become hypertrophic if the oxygen tension is high and the mechanical strain low. Finally, based on previous studies,[11,20] it was assumed that the cartilage subjected to chondrogenic conditions (specifically a low oxygen tension) for a period of 10 weeks formed stable cartilage. This stable cartilage inhibited blood vessel growth and was resistant to hypertrophy and endochondral ossification.

In accordance with the experimental model, tissue formation was predicted over 12 weeks, where each iteration of the model represented a 24-h period. In the empty defect model, it was assumed that the defect was filled with granulation tissue, which contained BMSCs. In the model of the defect treated with an engineered cartilage template, on implantation it was assumed that the encapsulated BMSCs had undergone chondrogenic differentiation for 32 days (equivalent to the preculture period described above). For this reason, in this model, the defect was assumed to be filled with chondrocytes at day 0.

Statistical analysis

Results are presented as mean ± standard deviation. Statistical analysis was performed with GraphPad Prism 5 software package (GraphPad). Experimental groups were analyzed for significant differences using either a *t*-test or a general linear model for ANOVA (analysis of variance). Significance was accepted at a level of $p < 0.05$.

Results

RGD-functionalized, γ-irradiated alginate hydrogels support the development of a cartilage template in vitro

Over 32 days of *in vitro* culture, the RGD-functionalized and γ-irradiated alginate hydrogels supported the development of a cartilage-like tissue that stained positive for collagen type II and sGAG deposition (Fig. 2c). sGAG and

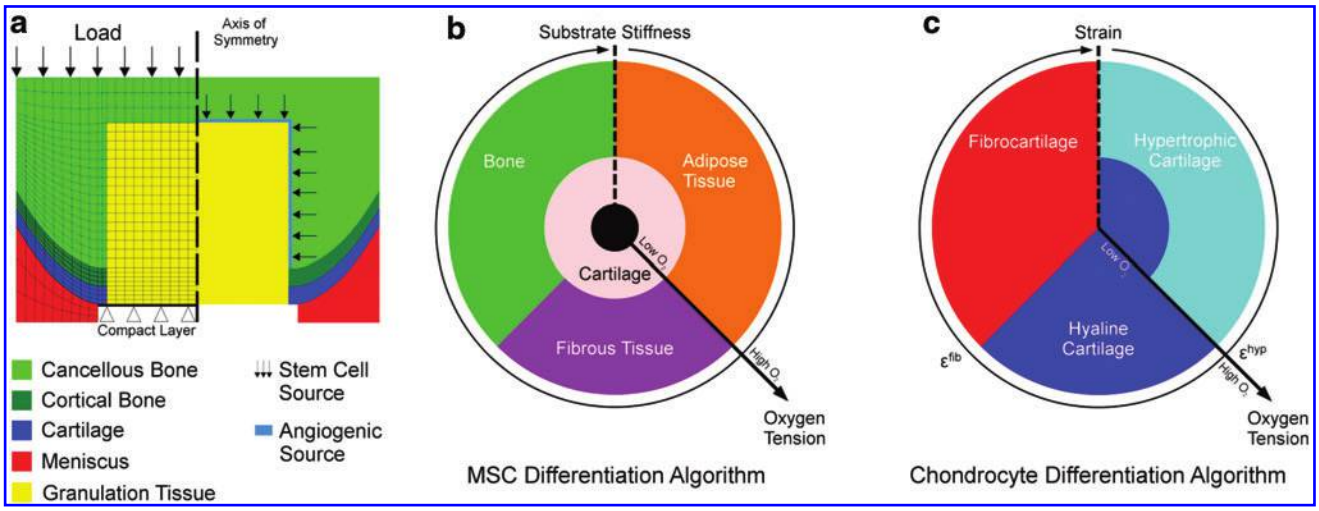

FIG. 1. FE model geometry and boundary conditions of an osteochondral defect for the simulations of the spontaneous repair process and tissue formation following implantation of the tissue-engineered scaffold **(a)**, tissue differentiation algorithm where **(b)** MSC fate is governed by a combination of the substrate stiffness and local oxygen tension,[51] and **(c)** chondrocyte fate is governed by the octahedral shear strain and local oxygen tension.[33] FE, finite element; MSC, mesenchymal stem cell. Color images are available online.

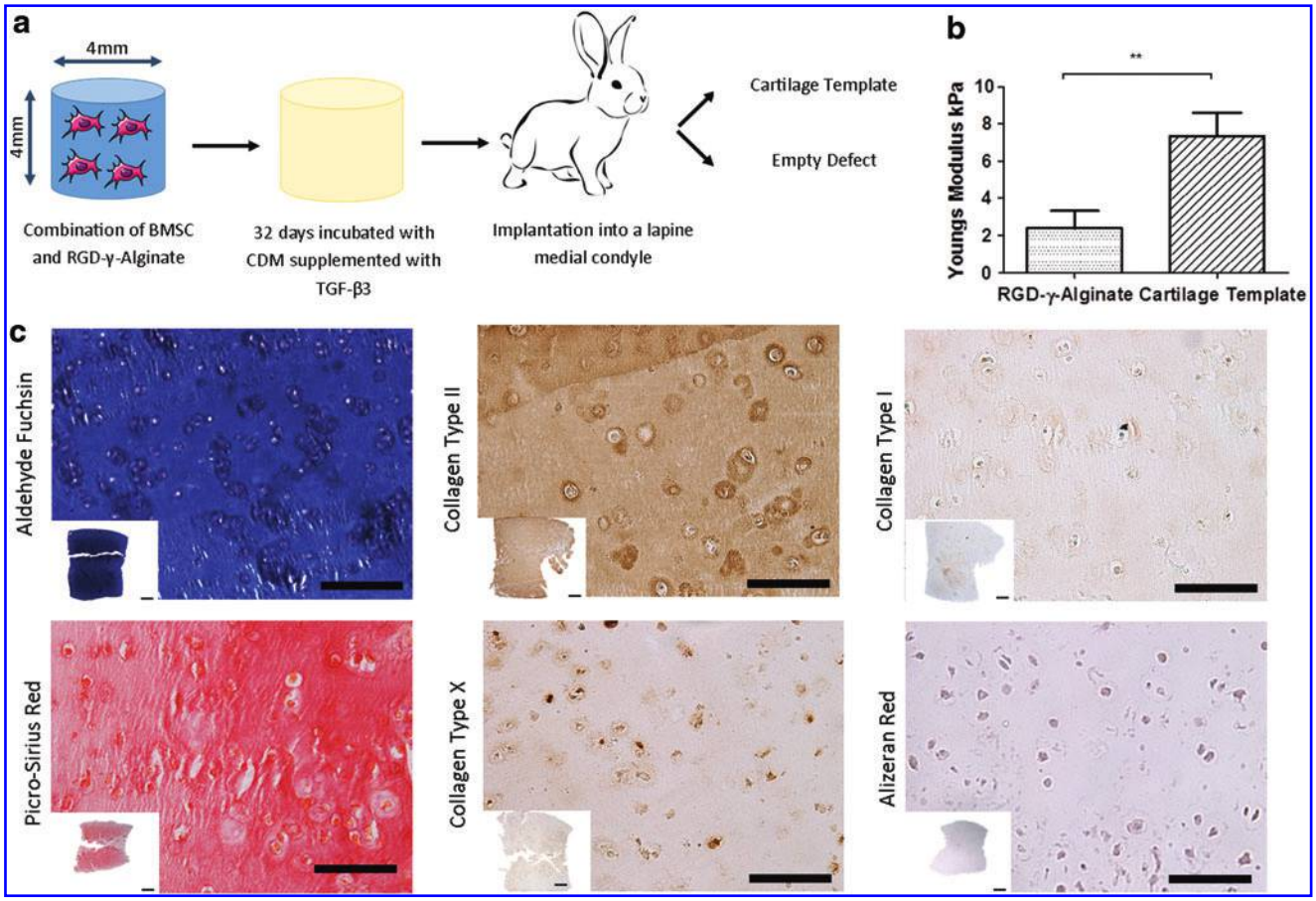

FIG. 2. **(a)** The process by which the cartilage template was formed, **(b)** Young's modulus for the acellular RGD-γ-alginate day 0 and after 32 days in culture preimplantation, $n = 3$ $^{**}p < 0.01$. **(c)** Histology for chondrogenic markers sGAG (alcian blue/aldehyde fuchsin), collagen (picrosirius red), and collagen type II, hypertrophic marker collagen type X, fibrocartilage collagen type I, and calcium (alizarin red), scale bar = 100 μm, *insert* scale bar = 1000 μm. RGD, arginine/glycine/aspartic acid; sGAG, sulfated glycosaminoglycan. Color images are available online.

collagen accumulation was measured to be 166 ± 28 and 123 ± 10 μg, respectively. There was some positive staining for collagen type X, indicating the early stages of hypertrophy in some areas of the cartilage template (Fig. 2c), although negative staining for alizarin red (for calcium deposition) and collagen type I demonstrated that the tissue had not ossified to any extent *in vitro* (Fig. 2c). There was a significant increase in mechanical properties of the template over time in culture, from 2.39 ± 0.94 to 7.35 ± 1.25 kPa (Fig. 2b). Live/dead analysis was conducted at the end of the culture period, which showed a cell viability of 84% within the cartilage templates (data not shown).

Treatment of OC defects with an engineered cartilage template results in the development of a stiffer repair tissue

Macroscopically, there was no difference apparent between the treated group and empty control group (Fig. 3a, b), as quantified using macroscopic scoring (Fig. 3c, d). In both groups, there were instances of what appeared to be both complete and partial filling of the defects. However, mechanical testing identified that repair tissue was significantly stiffer in defects treated with the cartilage template compared with empty controls (Fig. 3e–g).

De novo bone tissue, as measured by μCT, was observed within the OC defects. The reconstructed 3D scans demonstrated mineralized tissue within the center of the defect, with trabecular struts evident in the deeper regions of the repair tissue (Fig. 4a, b). Complete bone repair was not detected in either the empty or treated defects, and even in the best examples of repair there was some evidence of incomplete subchondral bone regeneration at the bone/cartilage interface. Quantitative analysis of the defect area revealed no significant difference in overall levels of bone fill between empty and treated defects (Fig. 4c, d).

Engineered cartilage templates promote the development of a more hyaline cartilage-like repair tissue in OC defects

All defects treated with engineered cartilage templates stained intensely with alcian blue, indicating the development of proteoglycan-rich tissue, with more variable staining observed within the empty controls (Fig. 5a, b). The best repair observed in the empty defects was fibrocartilaginous in nature, staining positively for type I and type II collagen, while the corresponding cartilage template-treated defects displayed a more hyaline-like tissue with only minimal type I collagen staining (Fig. 5a–d). The repair tissue stained weakly for type X collagen, a marker for hypertrophy, in the best repair for both empty and treated defects. However, there appeared to be pericellular staining for collagen type X in the empty defects that underwent poorer repair. Following blind evaluation of histological sections, a significant difference was found in the overall histological scores of empty and treated defects, with superior repair observed in treated defects (Fig. 6a, b). In addition, a lack of cellular alignment is observed within the empty

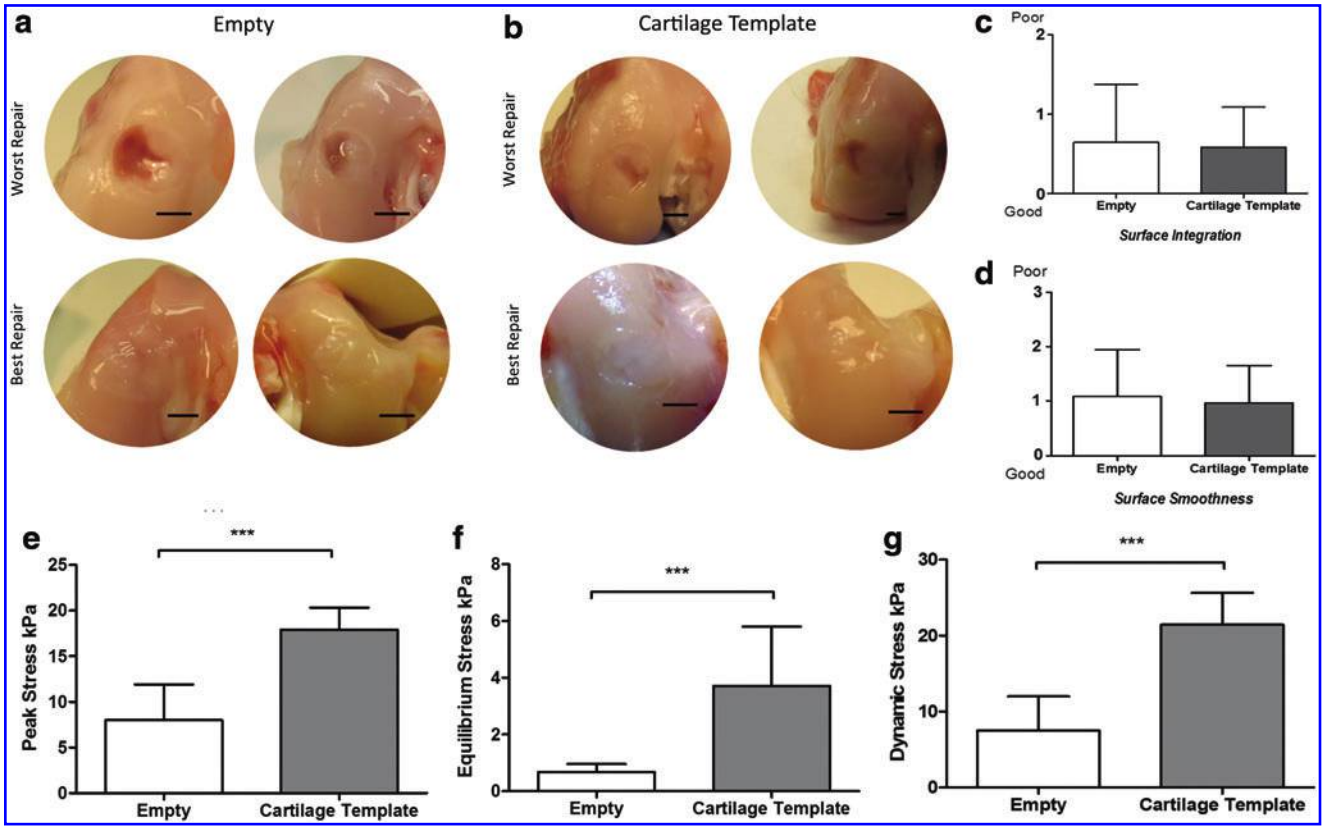

FIG. 3. Macroscopic repair of best and worst for **(a)** control empty defects and **(b)** cartilage template, scale bar = 2000 μm. Macroscopic scoring ($n = 6$) for **(c)** surface integration and **(d)** surface smoothness. **(e–g)** Mechanical testing at 3 months ($n = 6$ ***$p < 0.001$, **$p < 0.01$, *t*-test). Color images are available online.

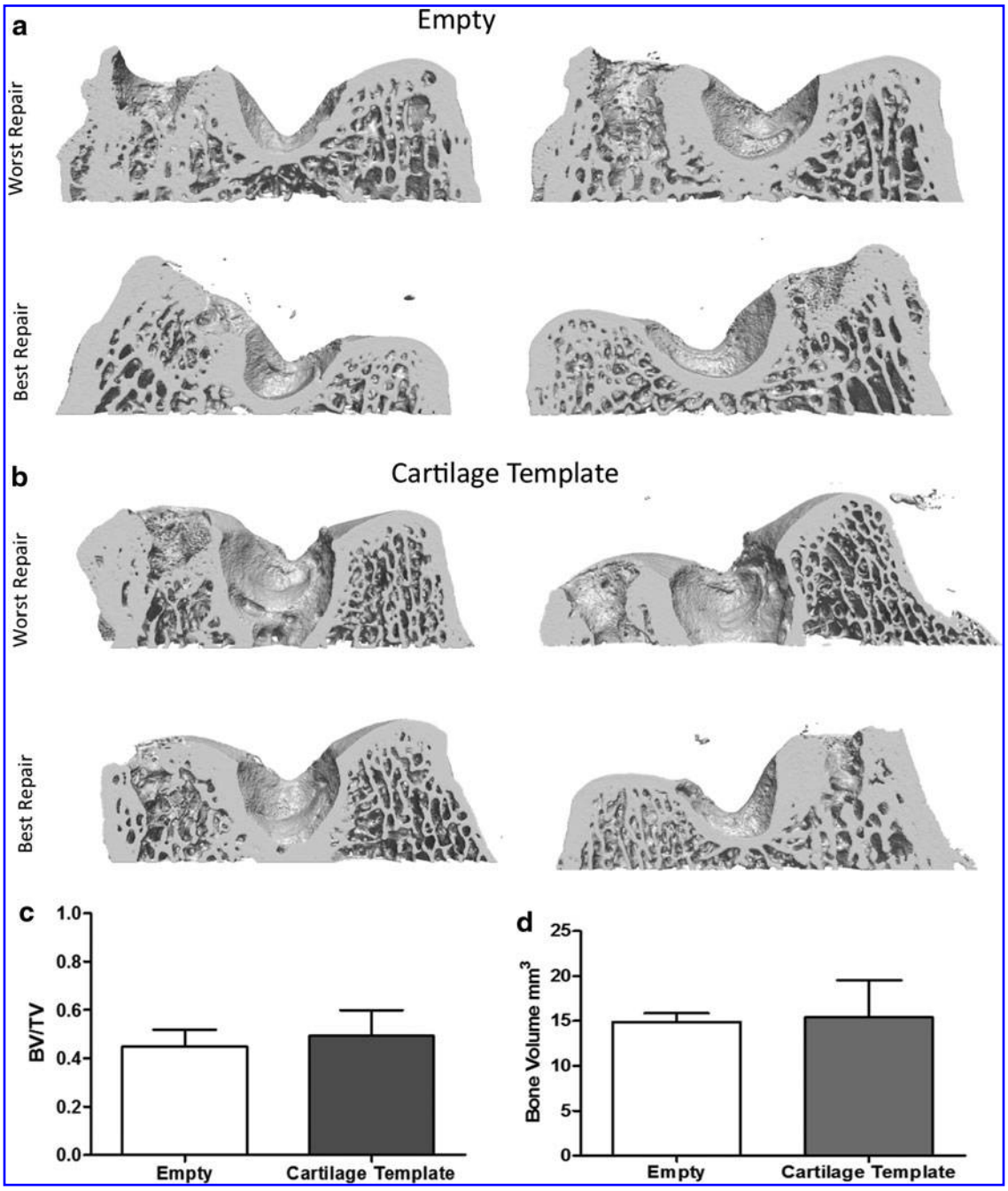

FIG. 4. Three-dimensional reconstruction of the microcomputed tomography scans of the **(a)** empty defects and **(b)** defects treated with cartilage templates. The *insert* image in the *top-left* of each shows the cross-sectional plane through the defect. Quantitative analysis of **(c)** the ratio of bone volume to total volume within a defined cylinder within the defect site and **(d)** total bone volume (scale bar = 4 mm).

controls when compared with native cartilage. The cartilage template-treated group generally exhibited normal cell morphology and alignment more like that of native articular cartilage (Fig. 5d). Overall, the histomorphometric analysis demonstrated that the cartilage template trended toward improved repair in all parameters evaluated, with significant differences observed for percentage tissue that is hyaline (Fig. 6b), integration of newly formed cartilage with surrounding cartilage (Fig. 6f), and a lack of degenerative changes in the adjacent tissue (Fig. 6h).

Computational predictions suggest that local levels of oxygen availability and mechanical stimuli may play a role in determining whether hyaline, fibrocartilage, or hypertrophic cartilage forms within OC defects

The computational mechanobiological model predicted the same patterns of tissue development as observed experimentally in both empty and treated defects. In models of both empty and treated defects, bone and cartilage were predicted to initially form in the osseous phase, while a

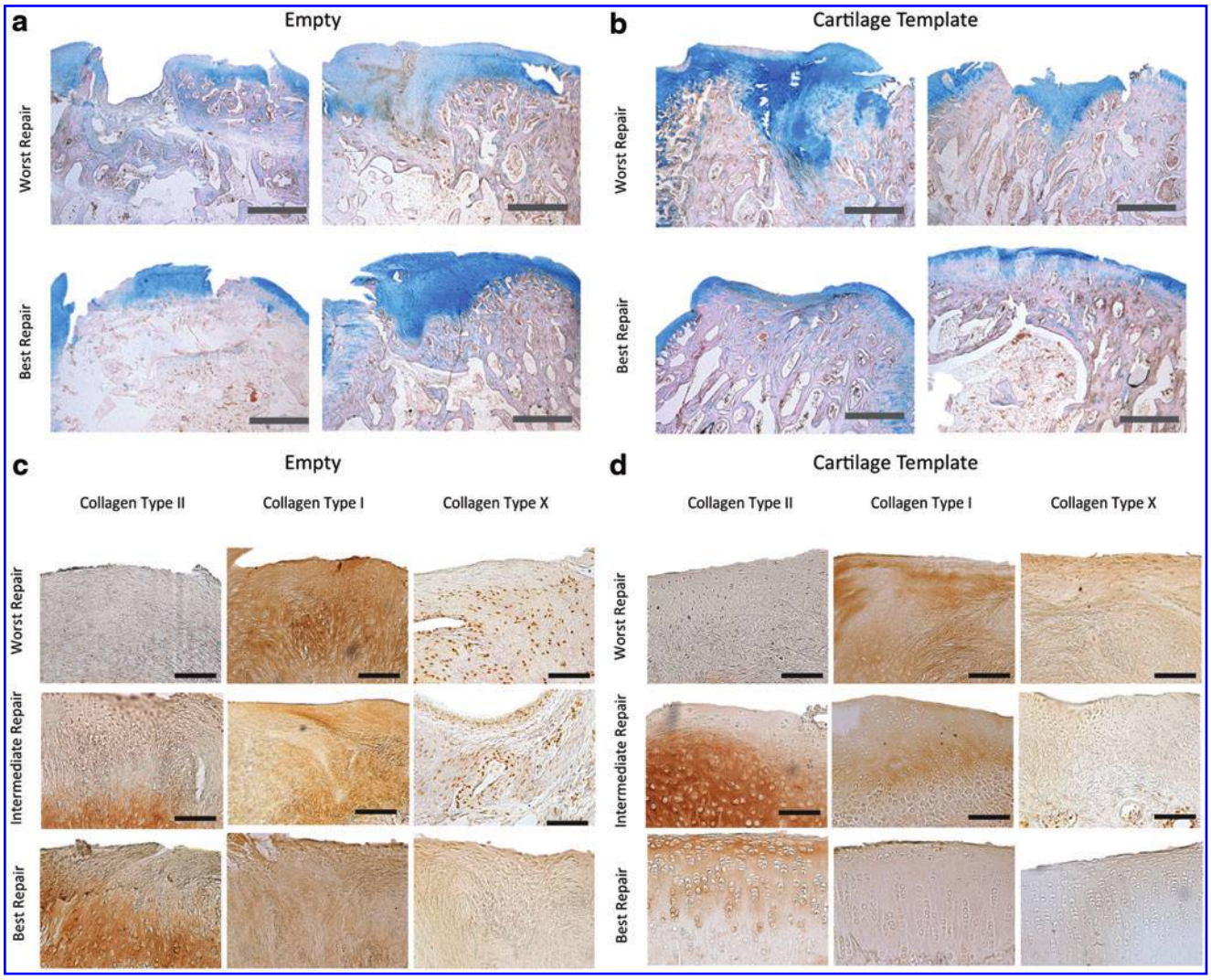

FIG. 5. Alcian blue staining depicting the two best and two worst observed repair for two different **(a)** empty and **(b)** cartilage templates (scale bar 2 mm). Immunohistochemical staining for collagen type II, I, and X portraying the worst, intermediate, and best repair for **(c)** empty and **(d)** cartilage templates (scale bar 200 μm). Color images are available online.

mixture of cartilage and fibrocartilage formed in the chondral phase of the defect (Fig. 7). As the simulations progressed, in both groups, a bone front advanced toward the chondral phase by means of endochondral ossification (Fig. 7b). Similar to the experimental findings, a higher quantity of cartilage was predicted at each time point in the chondral phase of defects treated with engineered templates (Fig. 7c). Conversely, in the empty defect simulation, a higher quantity of fibrocartilage was predicted in the chondral phase at each time point. In both models, there was roughly the same quantity of bone predicted in the osseous phase of the defect at weeks 4, 8, and 12 (Fig. 7d).

Similar patterns of bone formation predicted in the models can be attributed to the fact that there was very little difference in the spatial and temporal patterns of blood vessel formation predicted in empty and treated defects (Fig. 7a). In both models, blood vessels sprouted formed from the cancellous bone and, over time, advanced toward the surface of the defect. These similarities in the pattern of vessel formation resulted in a similar oxygen profile in empty and treated defects (Fig. 7a), which in turn supported comparable levels of osteogenesis.

The differences in the tissues formed in the chondral phase of the OC defect can be attributed, in part, to the higher stiffness of the engineered template compared with the granulation tissue that is assumed to initially fill the empty defect. The result of this was that the cells within the chondral phase of the scaffold-treated defect were subjected to lower magnitudes of strain compared with in the empty defect (data not shown). This, coupled with the hypoxic environment, supported higher levels of cartilage development compared with more fibrocartilage repair in empty defects. The greater persistence of cartilage within the chondral phase of the treated defects can be attributed to the preculture stage. This ensured that more stable cartilage (BMSCs chondrogenically stimulated for 32 days) had formed within the chondral phase of the treated defects compared with the empty defects. The result of this was

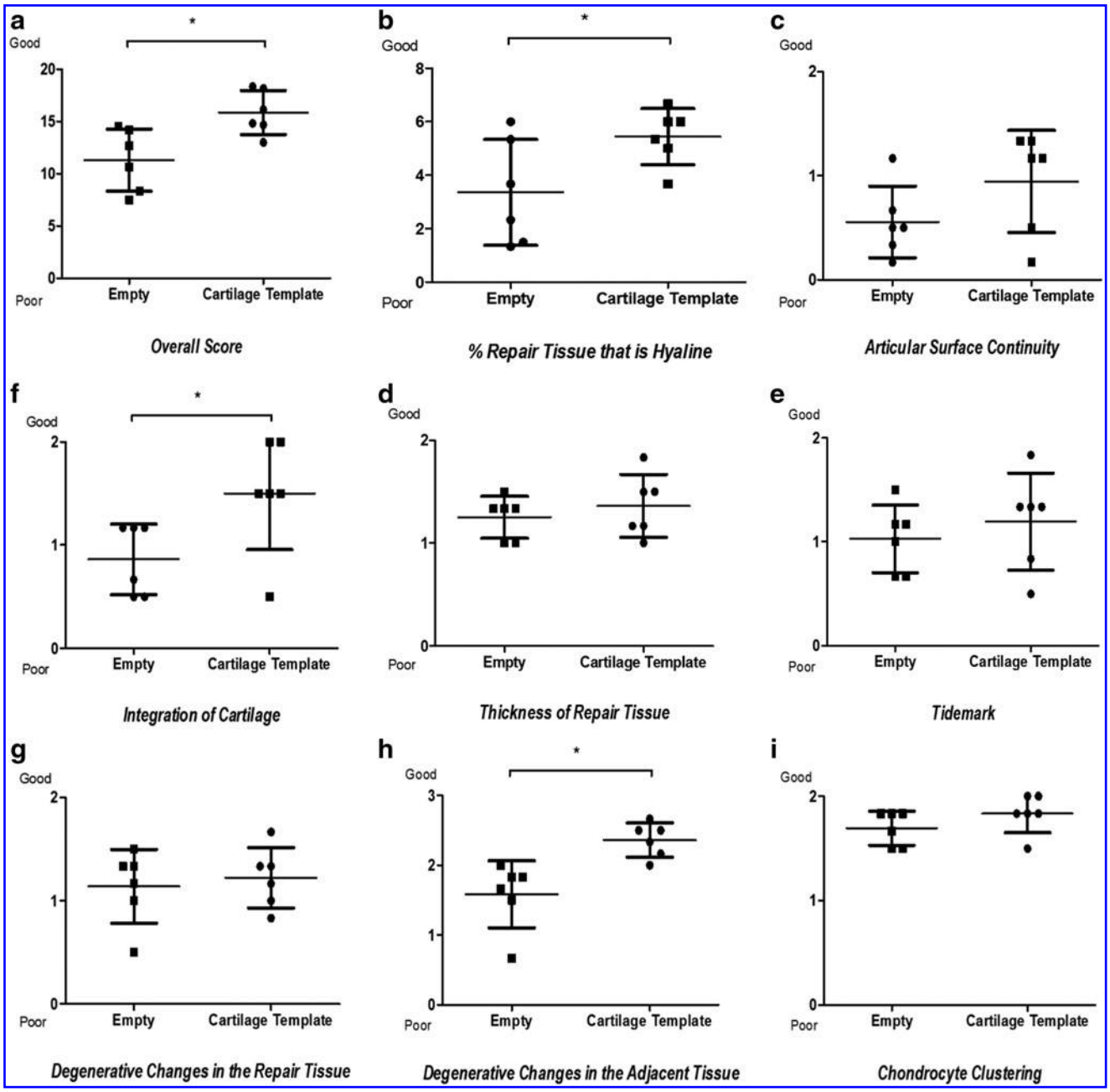

FIG. 6. Histomorphometric analysis of cartilage repair parameters, demonstrating significant differences in **(a)** overall score, **(b)** % hyaline repair tissue, **(c)** articular cartilage continuity, **(d)** thickness of repair tissue, **(e)** tidemark, **(f)** integration of cartilage, **(g)** degenerative changes in the repair tissue and **(h)** lack of degenerative changes to adjacent cartilage, **(i)** chondrocyte clustering ($n=6$, $*p<0.05$, t-test).

that, as blood vessels advanced toward the chondral phase, the cartilage in the treated defect was more resistant to hypertrophy and endochondral ossification.

Discussion

The OC unit develops postnatally from a cartilaginous precursor that undergoes endochondral ossification during skeletal maturation.[6,63] Inspired by this developmental process, herein we demonstrate that cartilaginous templates engineered using BMSCs encapsulated within RGD-modified and gamma-irradiated alginate hydrogels can be used to regenerate critically sized OC defects. While empty OC defects are capable of undergoing spontaneous repair,[64,65] more hyaline-like cartilage tissue was observed in defects treated with engineered soft tissue templates. Furthermore, the repair tissue in treated defects was stiffer than in empty controls. To provide a more mechanistic understanding of the regenerative process, we next used a computational model to simulate tissue development in both the empty and treated defects. This model provides evidence demonstrating that local levels of oxygen availability and

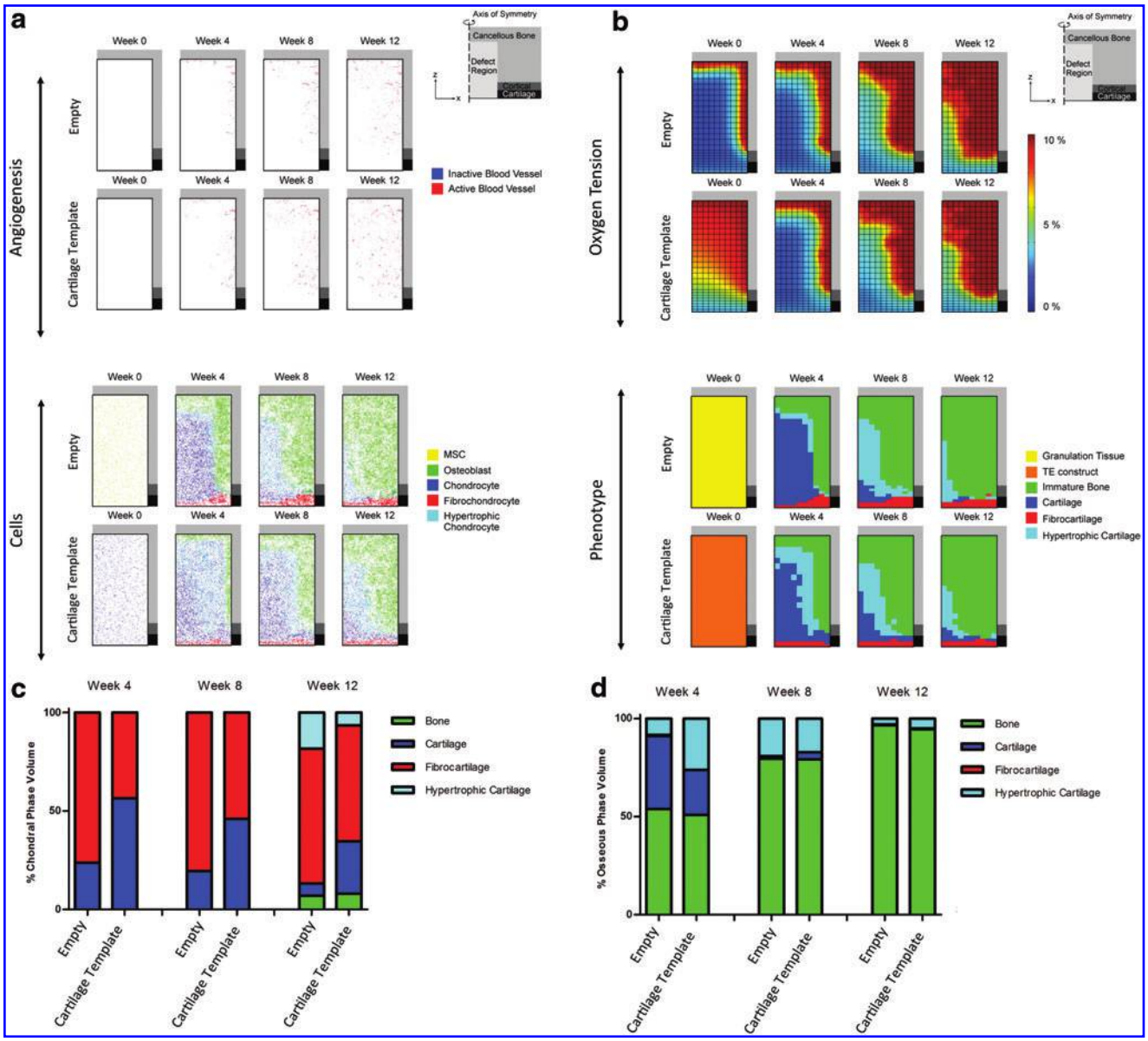

FIG. 7. **(a)** Spatial and temporal predictions of angiogenesis and cell differentiation within an empty defect and defect treated with the cartilage template. **(b)** Spatial and temporal predictions of oxygen tension and tissue phenotype. The relative volume of the different tissue phenotypes predicted within **(c)** the chondral phase and **(d)** the osseous phase of the defect. Color images are available online.

mechanical cues direct the fate of chondrogenically primed BMSCs following implantation into an OC defect.

Cartilage templates were engineered *in vitro* by encapsulating BMSCs within RGD-modified and γ-irradiated alginate hydrogels and by stimulating these constructs with TGF-β3 over 32 days *in vitro*. Such alginate hydrogels have previously been shown to support endochondral bone formation subcutaneously,[14] and in this study, cartilaginous tissues engineered within these gels also facilitated bone regeneration and remodeling within the osseous phase of the OC defect. Biomaterials are commonly used for bone tissue engineering; however, a key factor is tailoring the material degradation rate to synchronize with tissue formation and to facilitate vascular invasion. We have previously shown that unmodified alginate can support the development of a hypertrophic cartilage template *in vitro*[66] and endochondral bone formation subcutaneously,[16] but permitted only limited bone formation *in vivo* in a cranial defect model due to the slow degradation rate of the hydrogel.[39] However, using this modified alginate, in five of the six defects, there was no evidence of any residual material 3 months postimplantation.

Defects treated with the engineered cartilage template were found to contain a more hyaline-like repair tissue as demonstrated by histological staining, superior mechanical properties, and statistically significant histomorphometric scores. The inferior mechanical properties of the repair tissue within the empty control defects, coupled with positive collagen type I staining, suggest the development of a fibrocartilaginous tissue. The integration of the *de novo*

cartilage with existing cartilage is also paramount for joint stability, and is often reported to be difficult to achieve with bioengineering strategies.[67,68] For example, integration with the host tissue was one of the limiting factors reported to affect complete repair of OC defects using bone marrow-derived stem cells in a collagen gel.[68] In this study, we observe a significantly better integrated repair tissue in the treated group; however, consistent integration with the host cartilage was not obtained. In addition, we did not observe hyaline repair in all treated defects, demonstrating that further optimization of the tissue engineering strategy is warranted.

The computational models demonstrated that both the oxygen and mechanical environments varied spatially within the defect region, with higher levels of oxygen and lower magnitudes of strain leading to the prediction of endochondral bone formation in the osseous region of the defect, which correlated closely with our *in vivo* findings. Furthermore, the model suggested that local levels of oxygen availability and mechanical stimuli play a key role in determining whether hyaline, fibrocartilage, or hypertrophic cartilage would form in the chondral region of the defect. The improvement in cartilage formation observed in the treated group compared with the empty defects can be attributed to the increased stiffness of the engineered tissue when compared with granulation tissue, as well as the chondrogenic priming of the MSCs before implantation. The preculture period ensured that stable cartilage formed within the chondral phase of the scaffold at an earlier time point compared with the empty defect. This stable cartilage was hence more resistant to vascularization, hypertrophy, and endochondral ossification.

The insight provided by the *in silico* model can also be used to improve future tissue engineering strategies targeting larger and hence more challenging chondral, OC defects or whole-joint resurfacing applications. Ideally, the mechanical properties of the engineered template would more closely mimic that of the native tissue before implantation, or the oxygen environment within the template could be altered through the incorporation of hypoxia-inducing factors.[69] Potentially, a stiffer implant is required to sustain the harsh loading, however, it must not compromise the chondrogenic capacity of the implant. This could be achieved, for example, using the 3D biofabrication technology to reinforce the alginate hydrogel with printed polymer fibers.[70] Polycaprolactone-based scaffolds have previously been used in the repair of articular cartilage defects to some degree of success.[71]

In summary, tissue-engineered cartilage templates were found to undergo spatially defined differentiation in response to local environmental cues within OC defects. This engineered template prompted the development of a more hyaline-like cartilage repair tissue, pointing to the potential for developmentally inspired soft tissue templates, engineered using BMSCs, to regenerate damaged and diseased synovial joints.

Acknowledgments

Science Foundation Ireland grant number 12/IA/1554. We would also like to acknowledge the support of staff within the Comparative Medicine Unit in Trinity College Dublin for their help with the rabbit model.

Disclosure Statement

No competing financial interests exist.

References

1. Nakagawa, Y., Suzuki, T., Kuroki, H., Kobayashi, M., Okamoto, Y., and Nakamura, T. The effect of surface incongruity of grafted plugs in osteochondral grafting: a report of five cases. Knee Surg Sport Traumatol Arthrosc **15,** 591, 2007.
2. Bowland, P., Ingham, E., Jennings, L., and Fisher, J. Review of the biomechanics and biotribology of osteochondral grafts used for surgical interventions in the knee. Proc Inst Mech Eng H **229,** 879, 2015.
3. Koh, J.L., Wirsing, K., Lautenschlager, E., and Zhang, L.O. The effect of graft height mismatch on contact pressure following osteochondral grafting: a biomechanical study. Am J Sports Med **32,** 317, 2004.
4. Martin, I., Miot, S., Barbero, A., Jakob, M., and Wendt, D. Osteochondral tissue engineering. J Biomech **40,** 750, 2007.
5. Grässel, S., and Lorenz, J. Tissue-engineering strategies to repair chondral and osteochondral tissue in osteoarthritis: use of mesenchymal stem cells. Curr Rheumatol Rep **16,** 452, 2014.
6. Hunziker, E.B., Kapfinger, E., and Geiss, J. The structural architecture of adult mammalian articular cartilage evolves by a synchronized process of tissue resorption and neoformation during postnatal development. Osteoarthritis Cartilage **15,** 403, 2007.
7. Scotti, C., Tonnarelli, B., Papadimitropoulos, A., *et al.* Recapitulation of endochondral bone formation using human adult mesenchymal stem cells as a paradigm for developmental engineering. Proc Natl Acad Sci U S A **107,** 7251, 2010.
8. Kronenberg, H.M. Developmental regulation of the growth plate. Nature **423,** 332, 2003.
9. Hu, D.P., Ferro, F., Yang, F., *et al.* Cartilage to bone transformation during fracture healing is coordinated by the invading vasculature and induction of the core pluripotency genes. Development **144,** 221, 2017.
10. Ng, J.J., Wei, Y., Zhou, B., *et al.* Recapitulation of physiological spatiotemporal signals promotes in vitro formation of phenotypically stable human articular cartilage. Proc Natl Acad Sci U S A **114,** 2556, 2017, 28228529.
11. Liu, K., Zhou, G.D., Liu, W., *et al.* The dependence of in vivo stable ectopic chondrogenesis by human mesenchymal stem cells on chondrogenic differentiation in vitro. Biomaterials **29,** 2183, 2008.
12. Mackay, A.M., Beck, S.C., Murphy, J.M., Barry, F.P., Chichester, C.O., and Pittenger, M.F. Chondrogenic differentiation of cultured human mesenchymal stem cells from marrow. Tissue Eng **4,** 415, 1998.
13. Farrell, E., van der Jagt, O.P., Koevoet, W., *et al.* Chondrogenic priming of human bone marrow stromal cells: a better route to bone repair? Tissue Eng Part C Methods **15,** 285, 2009.
14. Daly, A.C., Cunniffe, G.M., Sathy, B.N., Jeon, O., Alsberg, E., and Kelly, D.J. 3D bioprinting of developmentally inspired templates for whole bone organ engineering. Adv Healthc Mater **5,** 2353, 2016.
15. Dang, P.N., Herberg, S., Varghai, D., *et al.* Endochondral ossification in critical-sized bone defects via readily implantable scaffold-free stem cell constructs. Stem Cells Transl Med **6,** 1644, 2017.

16. Sheehy, E.J., Mesallati, T., Kelly, L., Vinardell, T., Buckley, C.T., and Kelly, D.J. Tissue engineering whole bones through endochondral ossification: regenerating the distal phalanx. Biores Open Access **4,** 229, 2015.
17. Vinardell, T., Sheehy, E.J., Buckley, C.T., and Kelly, D.J. A comparison of the functionality and in vivo phenotypic stability of cartilaginous tissues engineered from different stem cell sources. Tissue Eng Part A **18,** 1161, 2012.
18. Chen, S., Fu, P., Cong, R., Wu, H., and Pei, M. Strategies to minimize hypertrophy in cartilage engineering and regeneration. Genes Dis **2,** 76, 2015.
19. Sheehy, E.J., Buckley, C.T., and Kelly, D.J. Oxygen tension regulates the osteogenic, chondrogenic and endochondral phenotype of bone marrow derived mesenchymal stem cells. Biochem Biophys Res Commun **417,** 305, 2012.
20. Leijten, J., Georgi, N., Moreira Teixeira, L., van Blitterswijk, C.A., Post, J.N., and Karperien, M. Metabolic programming of mesenchymal stromal cells by oxygen tension directs chondrogenic cell fate. Proc Natl Acad Sci U S A **111,** 13954, 2014.
21. Luo, L., Thorpe, S.D., Buckley, C.T., and Kelly, D.J. The effects of dynamic compression on the development of cartilage grafts engineered using bone marrow and infrapatellar fat pad derived stem cells. Biomed Mater **10,** 055011, 2015.
22. Carroll, S.F., Buckley, C.T., and Kelly, D.J. Cyclic hydrostatic pressure promotes a stable cartilage phenotype and enhances the functional development of cartilaginous grafts engineered using multipotent stromal cells isolated from bone marrow and infrapatellar fat pad. J Biomech **47,** 2115, 2014.
23. Vinardell, T., Rolfe, B.A., Buckley, C.T., *et al.* Hydrostatic pressure acts to stabilize a chondrogenic phenotype in porcine joint tissue derived stem cells. Eur Cells Mater **23,** 121, 2012.
24. Lafont, J.E. Lack of oxygen in articular cartilage: consequences for chondrocyte biology. Int J Exp Pathol **91,** 99, 2010.
25. Kanichai, M., Ferguson, D., Prendergast, P.J., and Campbell, V.A. Hypoxia promotes chondrogenesis in rat mesenchymal stem cells: a role for AKT and hypoxia-inducible factor (HIF)-1alpha. J Cell Physiol **216,** 708, 2008.
26. Robins, J.C., Akeno, N., Mukherjee, A., *et al.* Hypoxia induces chondrocyte-specific gene expression in mesenchymal cells in association with transcriptional activation of Sox9. Bone **37,** 313, 2005.
27. Takahashi, K., Kubo, T., Kobayashi, K., *et al.* Hydrostatic pressure influences mRNA expression of transforming growth factor-beta 1 and heat shock protein 70 in chondrocyte-like cell line. J Orthop Res **15,** 150, 1997.
28. Ikenoue, T., Trindade, M.C.D., Lee, M.S., *et al.* Mechanoregulation of human articular chondrocyte aggrecan and type II collagen expression by intermittent hydrostatic pressure in vitro. J Orthop Res **21,** 110, 2003.
29. Steward, A.J., Thorpe, S.D., Vinardell, T., Buckley, C.T., Wagner, D.R., and Kelly, D.J. Cell-matrix interactions regulate mesenchymal stem cell response to hydrostatic pressure. Acta Biomater **8,** 2153, 2012.
30. Thorpe, S.D., Nagel, T., Carroll, S.F., and Kelly, D.J. Modulating gradients in regulatory signals within mesenchymal stem cell seeded hydrogels: a novel strategy to engineer zonal articular cartilage. PLoS One **8,** e60764, 2013.
31. Li, Z., Yao, S.J., Alini, M., and Stoddart, M.J. Chondrogenesis of human bone marrow mesenchymal stem cells in fibrin-polyurethane composites is modulated by frequency and amplitude of dynamic compression and shear stress. Tissue Eng Part A **16,** 575, 2010.
32. Li, Z., Kupcsik, L., Yao, S.J., Alini, M., and Stoddart, M.J. Mechanical load modulates chondrogenesis of human mesenchymal stem cells through the TGF-β pathway. J Cell Mol Med **14,** 1338, 2010.
33. Lee, K.Y., and Mooney, D.J. Alginate: properties and biomedical applications. Prog Polym Sci **37,** 106, 2012.
34. Wang, L., Shelton, R.M., Cooper, P.R., Lawson, M., Triffitt, J.T., and Barralet, J.E. Evaluation of sodium alginate for bone marrow cell tissue engineering. Biomaterials **24,** 3475, 2003.
35. Awad, H.A., Wickham, M.Q., Leddy, H.A., Gimble, J.M., and Guilak, F. Chondrogenic differentiation of adipose-derived adult stem cells in agarose, alginate, and gelatin scaffolds. Biomaterials **25,** 3211, 2004.
36. Daly, A.C., Critchley, S.E., Rencsok, E.M., and Kelly, D.J. A comparison of different bioinks for 3D bioprinting of fibrocartilage and hyaline cartilage. Biofabrication **8,** 045002, 2016.
37. Freeman, F.E., Allen, A.B., Stevens, H.Y., Guldberg, R.E., and McNamara, L.M. Effects of in vitro endochondral priming and pre-vascularisation of human MSC cellular aggregates in vivo. Stem Cell Res Ther **6,** 218, 2015.
38. Freeman, F.E., and Kelly, D.J. Tuning alginate bioink stiffness and composition for controlled growth factor delivery and to spatially direct MSC fate within bioprinted tissues. Sci Rep **7,** 17042, 2017.
39. Cunniffe, G.M., Vinardell, T., Thompson, E.M., *et al.* Chondrogenically primed mesenchymal stem cell-seeded alginate hydrogels promote early bone formation in critically-sized defects. Eur Polym J **72,** 464, 2015.
40. Simmons, C.A., Alsberg, E., Hsiong, S., Kim, W.J., and Mooney, D.J. Dual growth factor delivery and controlled scaffold degradation enhance in vivo bone formation by transplanted bone marrow stromal cells. Bone **35,** 562, 2004.
41. Venkatesan, J., Bhatnagar, I., Manivasagan, P., Kang, K.H., and Kim, S.K. Alginate composites for bone tissue engineering: a review. Int J Biol Macromol **72,** 269, 2015.
42. Alsberg, E., Anderson, K.W., Albeiruti, A., Franceschi, R.T., and Mooney, DJ. Cell-interactive alginate hydrogels for bone tissue engineering. J Dent Res **80,** 2025, 2001.
43. Kong, H.J., Kaigler, D., Kim, K., and Mooney, D.J. Controlling rigidity and degradation of alginate hydrogels via molecular weight distribution. Biomacromolecules **5,** 1720, 2004.
44. Boontheekul, T., Kong, H.J., and Mooney, D.J. Controlling alginate gel degradation utilizing partial oxidation and bimodal molecular weight distribution. Biomaterials **26,** 2455, 2005.
45. Alsberg, E., Kong, H.J., Hirano, Y., Smith, M.K., Albeiruti, A., and Mooney, D.J. Regulating bone formation via controlled scaffold degradation. J Dent Res **82,** 903, 2003.
46. O'Reilly, A., and Kelly, D.J. Unravelling the role of mechanical stimuli in regulating cell fate during osteochondral defect repair. Ann Biomed Eng.**44,** 3446, 2016.
47. O'Reilly, A., and Kelly, D.J. Role of oxygen as a regulator of stem cell fate during the spontaneous repair of osteochondral defects. J Orthop Res **34,** 1026, 2016.
48. Jeon, O., and Alsberg, E. Photofunctionalization of alginate hydrogels to promote adhesion and proliferation of human mesenchymal stem cells. Tissue Eng Part A **19,** 1424, 2013.

49. Jeon, O., Powell, C., Ahmed, S.M., and Alsberg, E. Biodegradable, photocrosslinked alginate hydrogels with independently tailorable physical properties and cell adhesivity. Tissue Eng Part A **16,** 2915, 2010.
50. Jeon, O., Powell, C., Solorio, L.D., Krebs, M.D., and Alsberg, E. Affinity-based growth factor delivery using biodegradable, photocrosslinked heparin-alginate hydrogels. J Control Release **154,** 258, 2011.
51. Ignat'eva, N.Y., Danilov, N.A., Averkiev, S.V., Obrezkova, M.V., Lunin, V.V., and Sobol', E.N. Determination of hydroxyproline in tissues and the evaluation of the collagen content of the tissues. J Anal Chem **62,** 51, 2007.
52. Olvera, D., Daly, A., and Kelly, D.J. Mechanical testing of cartilage constructs. Methods Mol Biol **1340,** 279, 2015.
53. O'Reilly, A., Hankenson, K.D., and Kelly, D.J. A computational model to explore the role of angiogenic impairment on endochondral ossification during fracture healing. Biomech Model Mechanobiol **15,** 1279, 2016.
54. O'Reilly, A., and Kelly, D.J. A computational model of osteochondral defect repair following implantation of stem cell laden multiphase scaffolds. Tissue Eng Part A **23,** 30, 2017.
55. Grover, D.M., Chen, A.A., and Hazelwood, S.J. Biomechanics of the rabbit knee and ankle: muscle, ligament, and joint contact force predictions. J Biomech **40,** 2816, 2007.
56. Gushue, D.L., Houck, J., and Lerner, A.L. Rabbit knee joint biomechanics: motion analysis and modeling of forces during hopping. J Orthop Res **23,** 735, 2005.
57. Sundaramurthy, S., and Mao, J.J. Modulation of endochondral development of the distal femoral condyle by mechanical loading. J Orthop Res **24,** 229, 2006.
58. Proffen, B.L., McElfresh, M., Fleming, B.C., and Murray, M.M. A comparative anatomical study of the human knee and six animal species. Knee **19,** 493, 2012.
59. Checa, S., and Prendergast, P.J. A mechanobiological model for tissue differentiation that includes angiogenesis: a lattice-based modeling approach. Ann Biomed Eng **37,** 129, 2009.
60. Burke, D.P., Khayyeri, H., and Kelly, D.J. Substrate stiffness and oxygen availability as regulators of mesenchymal stem cell differentiation within a mechanically loaded bone chamber. Biomech Model Mechanobiol **14,** 93, 2015.
61. Burke, D., Dishowitz, M., Sweetwyne, M., Miedel, E., Hankenson, K.D., and Kelly, D.J. The role of oxygen as a regulator of stem cell fate during fracture repair in TSP2-null mice. J Orthop Res **31,** 1585, 2013.
62. Burke, D.P., and Kelly, D.J. Substrate stiffness and oxygen as regulators of stem cell differentiation during skeletal tissue regeneration: a mechanobiological model. PLoS One **7,** e40737, 2012.
63. Worthley, D.L., Churchill, M., Compton, J.T., *et al.* Gremlin 1 identifies a skeletal stem cell with bone, cartilage, and reticular stromal potential. Cell **160,** 269, 2015.
64. Orth, P., Cucchiarini, M., Kaul, G., *et al.* Temporal and spatial migration pattern of the subchondral bone plate in a rabbit osteochondral defect model. Osteoarthritis Cartilage **20,** 1161, 2012.
65. Wei, X., and Messner, K. Maturation-dependent durability of spontaneous cartilage repair in rabbit knee joint. J Biomed Mater Res **46,** 539, 1999.
66. Mesallati, T., Sheehy, E.J., Vinardell, T., Buckley, C.T., and Kelly, D.J. Tissue engineering scaled-up anatomically shaped osteochondral constructs for joint resurfacing. Eur Cell Mater **30,** 163, 2015.
67. Obradovic, B., Martin, I., Padera, R.F., Treppo, S., Freed, L.E., and Vunjak-Novakovic, G. Integration of engineered cartilage. J Orthop Res **19,** 1089, 2001.
68. Wakitani, S., Goto, T., Pineda, S.J., *et al.* Mesenchymal cell-based repair of large, full-thickness defects of articular cartilage. J Bone Joint Surg Am **76,** 579, 1994.
69. Park, K.M., and Gerecht, S. Hypoxia-inducible hydrogels. Nat Commun **5,** 4075, 2014.
70. Visser, J., Melchels, F.P.W., Jeon, J.E., *et al.* Reinforcement of hydrogels using three-dimensionally printed microfibres. Nat Commun **6,** 6933, 2015.
71. Martinez-Diaz, S., Garcia-Giralt, N., Lebourg, M., *et al.* In vivo evaluation of 3-dimensional polycaprolactone scaffolds for cartilage repair in rabbits. Am J Sports Med **38,** 509, 2010.

Address correspondence to:
Daniel Kelly, PhD
Trinity Centre for Bioengineering
Trinity Biomedical Sciences Institute
Trinity College Dublin
Dublin 2
Ireland

E-mail: kellyd9@tcd.ie

Received: February 6, 2018
Accepted: June 5, 2018
Online Publication Date: December 26, 2018

This article has been cited by:

1. Rossana Schipani, Stefan Scheurer, Romain Florentin, Susan E Critchley, Daniel J Kelly. 2020. Reinforcing interpenetrating network hydrogels with 3D printed polymer networks to engineer cartilage mimetic composites. *Biofabrication* **12**:3, 035011. [Crossref]
2. Susan Critchley, Eamon J. Sheehy, Gráinne Cunniffe, Pedro Diaz-Payno, Simon F. Carroll, Oju Jeon, Eben Alsberg, Pieter A.J. Brama, Daniel J. Kelly. 2020. 3D printing of fibre-reinforced cartilaginous templates for the regeneration of osteochondral defects. *Acta Biomaterialia* . [Crossref]
3. Yechi Qin, Guifei Li, Chen Wang, Danqing Zhang, Lili Zhang, Haowei Fang, Shifeng Yan, Kunxi Zhang, Jingbo Yin. 2020. Biomimetic Bilayer Scaffold as an Incubator to Induce Sequential Chondrogenesis and Osteogenesis of Adipose Derived Stem Cells for Construction of Osteochondral Tissue. *ACS Biomaterials Science & Engineering* **6**:5, 3070-3080. [Crossref]
4. Gabriela S Kronemberger, Renata Akemi Morais Matsui, Guilherme Almeida Santos Castro Miranda, José Mauro Granjeiro, Leandra Santos Baptista. 2020. Cartilage and bone tissue engineering using adipose stromal/stem cells spheroids as building blocks. *World Journal of Stem Cells* **12**:2, 110-122. [Crossref]
5. Wuren Bao, Menglu Li, Yanyu Yang, Yi Wan, Xing Wang, Na Bi, Chunlin Li. 2020. Advancements and Frontiers in the High Performance of Natural Hydrogels for Cartilage Tissue Engineering. *Frontiers in Chemistry* **8**. . [Crossref]